Chemical Science International Journal

Volume 33, Issue 2, Page 25-45, 2024; Article no.CSIJ.113143
ISSN: 2456-706X
(Past name: American Chemical Science Journal, Past ISSN: 2249-0205)

Microscale Thermophoresis Analysis of Membrane Proteins

Nighat Nawaz [a,b], Roshan Ali [c], Muhammad Ali [c], Iain W. Manfield [d], Muhammad Kamran Taj [e], Mohammad Zahid Mustafa [e] and Simon G. Patching [a*]

[a] School of Biomedical Sciences (Astbury Building), University of Leeds, Leeds LS2 9JT, UK.
[b] Department of Chemistry, Islamia College Peshawar, Peshawar 25120, Pakistan.
[c] Institute of Basic Medical Sciences, Khyber Medical University, Peshawar 25100, Pakistan.
[d] School of Molecular and Cellular Biology, University of Leeds, Leeds LS2 9JT, UK.
[e] Centre for Advanced Studies in Vaccinology and Biotechnology, University of Balochistan, Quetta 08763, Pakistan.

Authors' contributions

This work was carried out in collaboration among all authors. All authors read and approved the final manuscript.

Article Information

DOI: 10.9734/CSJI/2024/v33i2887

Open Peer Review History:
This journal follows the Advanced Open Peer Review policy. Identity of the Reviewers, Editor(s) and additional Reviewers, peer review comments, different versions of the manuscript, comments of the editors, etc are available here: https://www.sdiarticle5.com/review-history/113143

Review Article

Received: 24/12/2023
Accepted: 28/02/2024
Published: 04/03/2024

ABSTRACT

Microscale thermophoresis (MST) is an analytical technique for measuring biomolecular interactions. It is based on the physical phenomenon that particles move within temperature gradients, which is affected by their size, charge, hydration shell and conformation. The MST sample must contain a fluorescent target molecule used to observe the movement of particles, and this can be titrated with an unlabelled binding partner for quantifying the interaction. MST is highly sensitive, using relatively small amounts of sample, and it has no limitations on the size of the target biomolecule, on the affinity of the interaction or on the composition of the buffer and other sample components. This makes MST ideally suited to characterising interactions with membrane

**Corresponding author: E-mail: s.g.patching@leeds.ac.uk, simonpatching@yahoo.co.uk;*

proteins, which can be studied in cell lysates, native membranes, solubilised in detergents or reconstituted in lipids. The intrinsic aromatic residues of membrane proteins have been used as the fluorophore for MST (label-free MST) or membrane proteins have been labelled with a range of fluorescent dyes or conjugated with fluorescent proteins (labelled MST). The different types of membrane proteins that have had biomolecular interactions characterised by MST include the SARS-CoV-2 spike protein, GPCRs and other receptors, sensor kinases, ion channels, aquaporins, and transport proteins.

Keywords: Biomolecular interactions; fluorescent labelling; ligand binding; drug screening; SARS-CoV-2 spike protein; GPCRs; receptors; ion channels; aquaporins; transport proteins.

1. INTRODUCTION

Microscale thermophoresis (MST) is a biophysical technique for measuring biomolecular interactions. It is based on the physical phenomenon that particles move within temperature gradients, usually from regions of higher to lower temperature. The movement of particles is affected by their size, charge, hydration shell and conformation, any of which can change during biomolecular interactions [1-14]. In MST a microscopic temperature gradient is induced by infrared (IR) laser light and the sample must contain a fluorescent target molecule that is used to observe the movement of particles. The fluorescent molecule is kept at a constant concentration and is titrated with a range of concentrations of an unlabelled binding partner. The movement of fluorescent molecules within the temperature gradient results in a quantifiable change in their local concentration and therefore of the measured fluorescence, thus enabling estimation of binding affinities and kinetic parameters [15-18]. The necessary fluorescence property may be intrinsic to one of the binding partners (e.g., from aromatic residues in a protein) (label-free MST) or a fluorescent dye or other fluorescent protein (e.g., green fluorescent protein, GFP) must be attached to one of the binding partners (labelled MST). MST can measure many types of biomolecular interactions, including protein-protein, protein-nucleic acid, protein-lipid, protein-small molecule/peptide/ion or protein-liposome/vesicle interactions. It can also measure conformation changes in a biomolecule that is subjected to varying conditions. In addition to binding affinities and kinetic parameters, MST can be used to assess other physical parameters of biomolecules and their interactions such as aggregation and precipitation, stoichiometry and oligomerisation.

2. THE MST EXPERIMENT

In the MST instrument (Fig. 1A), samples are measured in fine glass capillaries with a typical total volume of 4 µl. The capillary contains a solution of a fluorescent target molecule and a binding partner. The fluorescent molecule is excited using an appropriate wavelength of light and the emitted fluorescence is detected, both through the same objective lens. An IR laser is focused into the capillary to create a microscopic temperature gradient at the exact spot where fluorescence emission is detected. This gradient is focused on a diameter of around 50 µm and typically contains a temperature difference of 2-6 °C.

The MST experiment (Fig. 1B) begins with the IR laser switched off, where molecules are homogenously distributed and diffuse freely within the sample. At this point the initial fluorescence intensity is detected. When the IR laser is switched on there is immediate heating of the focused area resulting in a rapid change in fluorophore properties and a strong decrease in fluorescence intensity before thermophoresis begins. This is followed by thermophoretic movement of the fluorescent molecules out of the heated area resulting in a slow decrease in fluorescence intensity. A steady state is typically reached after around 30 seconds. The IR laser is then turned off resulting in an immediate increase in fluorescence intensity. As the sample cools down there is movement of fluorescent molecules back into the area that was heated to give a further increase in fluorescence intensity. For each sample, the normalised fluorescence (F_{norm}) is calculated from the initial fluorescence (F_0) and from the fluorescence after thermophoresis (F_1), as follows: $F_{norm} = F_1/F_0$. The change in the normalised fluorescence against the change in concentration of binding partner can be used to quantify the affinity of the binding interaction.

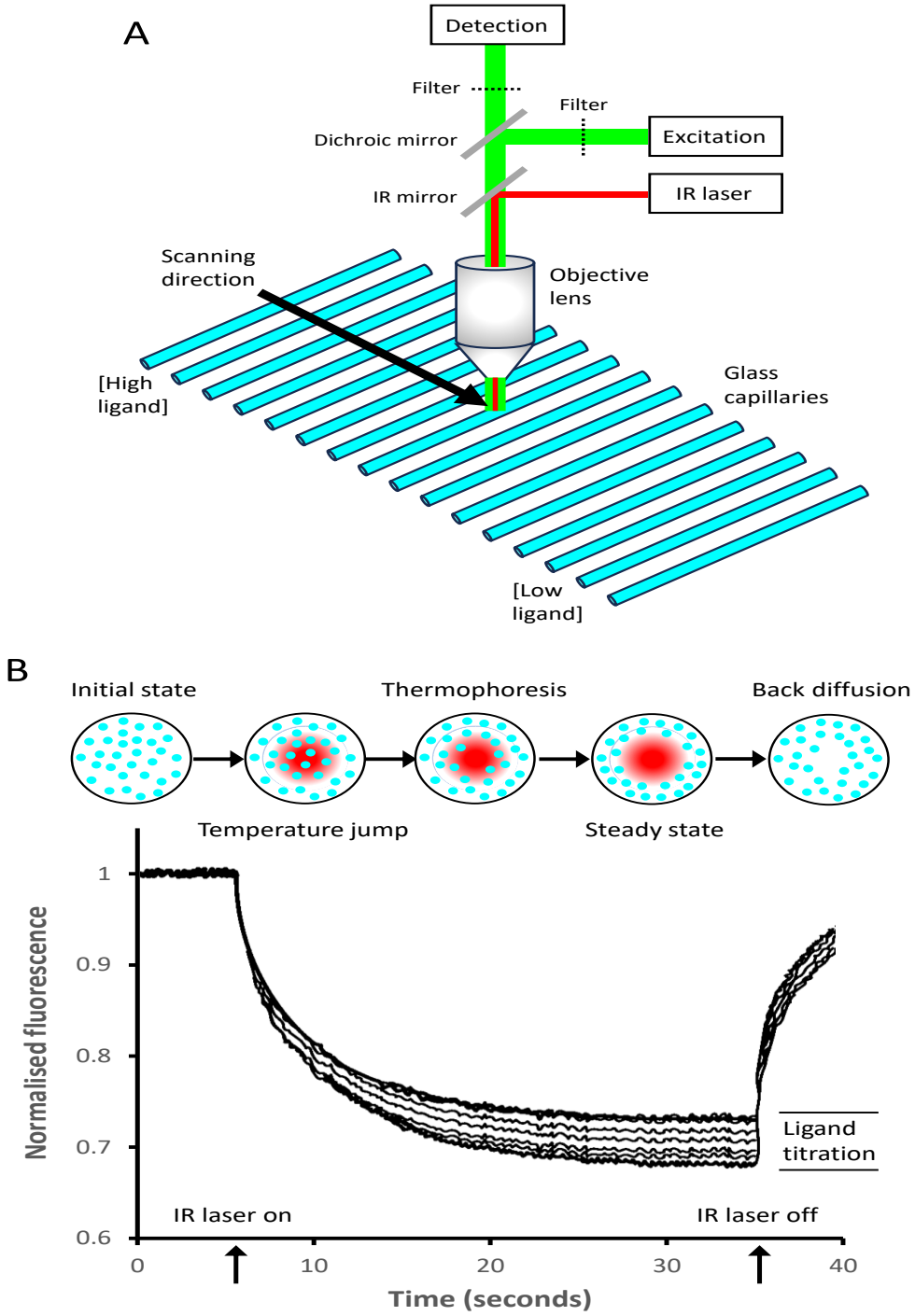

Fig. 1. The MST experiment

*In the MST instrument (**A**) a series of sixteen glass capillaries (volume 4 µl) are filled with samples containing a constant concentration of a fluorescent target biomolecule and a range of concentrations of a binding partner (e.g. a ligand). The samples are scanned in turn by being subjected to heating at a microscopic area (50 µm diameter) using an IR laser, which creates a temperature gradient. Fluorescence is measured at the same area to follow movement of the target biomolecules. In the profile of the MST experiment (**B**) the initial fluorescence is measured then the IR laser is turned on (5 seconds). This induces an immediate temperature jump and then movement of the target biomolecule away from the heated area (thermophoresis) takes place until a steady state is reached (~30 seconds). The IR laser is turned off (35 seconds) then there is back diffusion of the target biomolecule. The magnitude of the thermophoresis, and therefore the normalised fluorescence intensity, are altered by different concentrations of the ligand*

3. ADVANTAGES OF MST

MST is a relatively simple, robust, and rapid technique that has several advantages over other biophysical techniques commonly used to measure biomolecular interactions such as surface plasmon resonance (SPR) [19-23], isothermal titration calorimetry (ITC) [24-30], fluorescence spectroscopy [31, 32], circular dichroism (CD) spectroscopy [33-36], solution- and solid-state nuclear magnetic resonance (NMR) spectroscopy [37-50], and mass spectrometry (MS) [51-61]. MST has no limitations on the size of the target biomolecule or on the affinity of the interaction to be measured (pM to mM) or on the composition of the buffer and other sample components. The sample may contain detergents or lipids and MST measurements can be performed on complex samples such as cell lysates or membrane preparations. Unlike in SPR, the target biomolecule does not need to be immobilised. MST is highly sensitive, so a principal advantage is that experiments use relatively small amounts of sample. For example, a full titration using sixteen capillaries each containing 4 µl and performed in triplicate would use a total volume of 192 µl. This would contain a total of 1.92-19.20 picomoles of fluorescent biomolecule if at a concentration of 10-100 nM. It follows that assay optimisation also has low sample consumption. MST measurements in the instrument are relatively quick, taking around 40 seconds per sample/titration point, so a full titration with a series of sixteen dilutions can be run in under 15 minutes. These advantages mean that MST is particularly well suited to studying membrane proteins [62-64] that are often large and must be kept in a membrane, lipid or detergent environment to retain their native structure and activity, and some, especially eukaryotic proteins, can only be obtained in small quantities.

4. MST ANALYSIS OF MEMBRANE PROTEINS

When manipulating a membrane protein with a fluorophore for MST measurements, any potential effects of the fluorophore on the native structure and activity of the protein should be considered and tested for. This should include the use of appropriate controls in the MST measurements and may require the use of other biophysical and biochemical analyses to test structural integrity and activity. Such effects can be avoided if native aromatic residues in a target membrane protein can be used as the fluorophore for MST measurements, but only four of the studies on membrane proteins (4/60) employed this approach (Table S1). On the face of it use of native aromatic residues is more straightforward than reacting the target membrane protein with a fluorescent dye or conjugating it with a fluorescent protein, but the intensity of intrinsic fluorescence produced in most membrane proteins studied was presumably not high enough for efficient detection.

One strategy that avoids manipulating the target membrane protein with a fluorophore is to reconstitute it in nanodiscs that have themselves been reacted with a fluorescent dye. For example, MST measurements were performed on the human neurotensin receptor NTS1 reconstituted in nanodiscs formed using fluorescently labelled membrane scaffold protein MSP1D1. MST measured binding of the G-protein subunit Gαi1 to NTS1 in Alexa Fluor™ 647-labelled MSP1D1 nanodiscs formed using different lipids and in the presence of different NTS1 ligands. The affinity of Gαi1 binding to NTS1 was influenced by the lipid composition of the nanodiscs, where the highest affinities were obtained using porcine brain polar lipid (BPL) in the absence of ligand (K_D = 300 ± 100 nM) and in the presence of agonist neurotensin (K_D = 140 ± 60 nM). Empty nanodiscs (no NTS1) did have a similar binding affinity in the presence of neurotensin (K_D = 200 ± 100 nM). For comparison, affinities in the presence of antagonists SR48692 or SR142948A were 600 ± 300 nM and 300 ± 100 nM, respectively, and in the presence of a non-hydrolysable analogue of GTP (GTPγS) (negative control) the affinity was 1.5 ± 0.8 µM [65].

5. FLUOROPHORES USED IN MST MEASUREMENTS ON MEMBRANE PROTEINS

Out of the 60 different studies that have used MST to analyse membrane proteins (Table S1) over a half (52.5%) have employed commercial kits designed to be used with Monolith MST instruments. The majority of these kits were red (17/60) or blue (4/60) dyes containing a succinimidyl ester group that reacts with the primary amines on lysine residues to form a covalent bond. Some the of kits (8/60) were red dyes that react with His-tags engineered on to the target biomolecule, which can be used with

either purified proteins or crude samples (e.g. cell lysates). A few of the kits (2/60) were green dyes containing a maleimide reactive fluorophore that reacts with cysteine residues to form a covalent bond. All of these kits are generally optimised for proteins with a molecular weight of more than 5 kDa and concentrations of 2-20 µM. The next most common type of fluorophore used with membrane proteins were three Alexa Fluor™ dyes (488, 546, 647) (7/60) (Figure 2). Alexa Fluor™ 488 (**1**) is a bright green dye with excitation suited to the 488 nm laser line. Alexa Fluor™ 546 (**2**) is a bright orange dye that can be excited using 488 nm or 532 nm laser lines. Alexa Fluor™ 647 (**3**) is a bright far-red dye with excitation suited to the 633 nm laser line, it contains a succinimidyl ester group that can react with the primary amines of lysine residues. In some studies (4/60) the target membrane protein was conjugated to GFP, which can be excited by the 488 nm laser line. GFP from *Aequorea victoria* (water jellyfish) is comprised of 238 amino acids (26.9 kDa) (UniProt P42212) and has a β-barrel structure with eleven β-strands [66,67]. The chromophore of GFP consists of the three amino acids Ser-dehydroTyr-Gly (residues 65-67), which have been mutated (F64LT) to create enhanced GFP (eGFP) that has increased fluorescence intensity, greater photostability and higher efficiency compared to wild-type [68,69]. Three of the studies (3/60) used the dye Cy5 (1,1′-dimethyl-3,3,3′,3′-tetramethylindocarbocyanine) (**4**) as fluorophore (Figure 2), which is a far-red fluorescent dye with excitation suited to the 633 nm or 647 nm laser lines. Cy5 contains an amine group that can be reacted with activated esters and other electrophilic reagents. One study (1/60) used the zwitterionic red dye Atto-647 (**5**) as fluorophore (Fig. 2), for which suitable excitation sources are next to the He:Ne laser (633 nm), the 647 nm line of the Krypton-Ion laser or a diode-laser emitting at 650 nm.

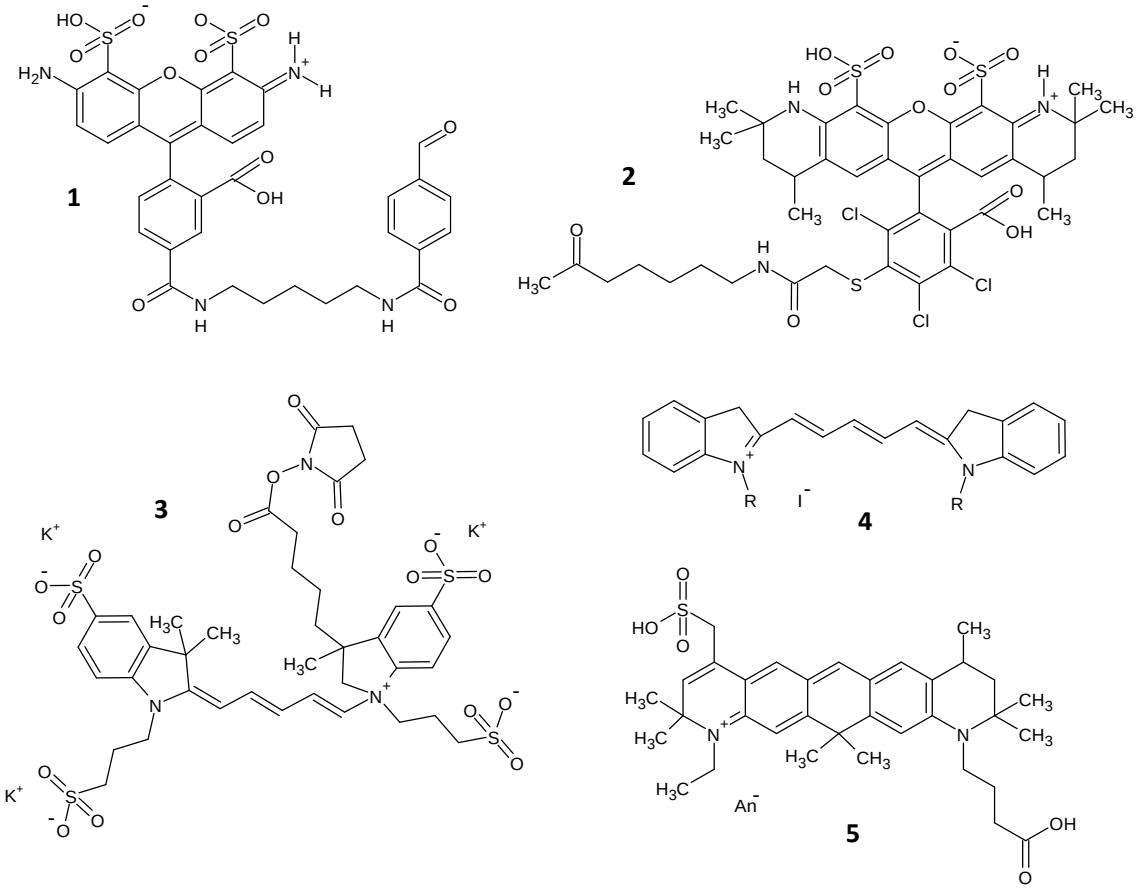

Fig. 2. Chemical structures of some fluorophores used in MST measurements on membrane proteins

Alexa Fluor™ 488 (1), Alexa Fluor™ 546 (2), Alexa Fluor™ 647 (3), Cy5 (4), and Atto-647 (5)

6. MEMBRANE PROTEINS ANALYSED BY MST

The different types of membrane proteins that have had biomolecular interactions characterised by MST include the severe acute respiratory syndrome coronavirus 2 (SARS-CoV-2) spike protein, GPCRs and other receptors, sensor kinases, ion channels, aquaporins, transport proteins, and others.

6.1 SARS-CoV-2 Spike Protein

In recent years eleven studies have employed MST to analyse various interactions with the SARS-CoV-2 spike protein, which binds to the angiotensin-converting enzyme 2 (ACE2) receptor on target human cells. MST was used to measure the binding of bacterial (*Escherichia coli*) lipopolysaccharide to the full-length (residues 16 to 1213) fluorescently-labelled SARS-CoV-2 spike protein, giving a K_D of 46.7 ± 19.7 nM [70]. Various techniques were used to investigate the molecular mechanism of how the SARS-CoV-2 spike protein augments lipopolysaccharide-mediated hyperinflammation, where the spike protein serves as a lipopolysaccharide delivery system to its receptors. This included use of MST to measure the binding affinity of lipopolysaccharide to the SARS-CoV-2 spike protein Wuhan variant (K_D = 46.7 ± 19.7 nM) and Omicron variant (K_D = 3.3 ± 1.5 µM), of lipopolysaccharide to Wuhan S1 (K_D = 50.0 ± 20.0 nM) and Omicron S1 (K_D = 4.6 ± 1.7 µM), and of lipid A to subunit Wuhan S1 (42.2 ± 24.4 nM) and Omicron S1 (K_D = 0.6 ± 0.2 µM). Binding of lipopolysaccharide to Wuhan S2 (K_D = 3.6 ± 1.6 µM) had a weaker affinity than for S1 [71].

In a study that used machine learning models to identify inhibitors of SARS-CoV-2 through the repurposing of existing drugs, MST was used to measure binding of the antimalarial drug lumefantrine to the SARS-CoV-2 spike protein receptor binding domain (RBD). Residues 331 to 528 of the spike protein were expressed and purified and labelled with the amine reactive dye RED-NHS. Titration of lumefantrine with the spike protein RBD produced a K_D of 259 ± 78 nM [72]. MST measured binding of the fungal defensin micasin from *Microsporum canis* to the spike protein RBD. The latter was labelled with the fluorescent dye NT−495−NHS and in MST experiments titrated with wild-type micasin and some mutant forms. Micasin bound to the spike protein RBD with a K_D of 5.04 ± 0.96 µM [73]. A study used various computational and experimental approaches to identify molecules that could be optimised to improve anti-SARS-CoV-2 activity. Five beta-blockers (pindolol, carvedilol, carteolol, atenolol, and bisoprolol) against the SARS-CoV-2 spike protein RBD were identified. The highest affinity of these was carvedilol, for which MST measured a K_D value of 364 ± 22 nM [74]. In a study that designed high-affinity affibody ligands for purification of the RBD from coronavirus spike proteins, MST was used to measure binding of ZRBD-02 (K_D = 133.4 nM), ZRBD-04 (K_D = 377.3 nM), and ZRBD-07 (K_D = 36.3 nM) to the SARS-CoV-2 spike protein RBD [75].

One of the studies designed and tested six synthetic ACE2-based peptides to antagonise the interaction between ACE2 and the spike protein RBD based on molecular docking with crystal structures of their interface. The ability of the peptides to inhibit the ACE2-spike-RBD interaction was tested using a luciferase assay, then the affinity of peptide binding to the spike-RBD protein was measured by MST. The purified spike-RBD protein was fluorescently labelled and incubated with each peptide at a range of concentrations (12.5–0.00019 µM). Some of the peptides had binding affinities in the low nanomolar range, with the highest affinity peptides having K_D values of 13 and 45 nM [76]. In a different study synthetic α-helical peptides mimicking the α1-helix motif of the ACE2 receptor were tested as potential inhibitors of the ACE2 SARS-CoV-2 interaction. A series of peptides N-capped with either Ac-βHAsp-[ProM-5] or Ac-βHAsp-PP were tested and MST measurements demonstrated a strong binding affinity (K_D = 62 nM) of an Ac-βHAsp-PP-capped peptide for the SARS-CoV-2 spike protein RBD [77]. MST was used to confirm how C-2 thiophenyl tryptophan trimers inhibit cellular entry of SARS-CoV-2 through interaction with the spike protein. MST measured binding of compounds to the spike protein and to its RBD, and also the effect of the compounds on interaction of the spike protein and its RBD with ACE2 [78]. Following a study to measure differential interactions between human ACE2 and the spike RBD of SARS-CoV-2 variants of concern [79], a later study used a combination of steered molecular dynamics (SMD) simulation and experimental MST to quantify the interaction between the Omicron variant of the RBD and human ACE2 [80]. MST measurements of binding between human ACE2 and different mutants of the RBD were directed by the SMD

simulation. It was identified that Omicron produces an enhanced RBD-ACE2 interaction through mutations N501Y, Q498R and T478K in the RBD. The Omicron variant of the RBD had a five-fold higher affinity for ACE2 (K_D = 5.5 ± 1.4 nM) than did the wild-type RBD (K_D = 27.5 ± 4.8 nM), and higher affinities than the RBDs of the Alpha (K_D = 11.8 ± 0.8 nM), Beta (K_D = 23.1 ± 2.4 nM) and Delta (K_D = 21.5 ± 2.9 nM) variants [80].

6.2 G Protein-Coupled Receptors

Nine studies have employed MST to analyse binding interactions to different GPCRs. In a study that reported structure and function analyses of the purified GPCR human vomeronasal type 1 receptor 1, MST using native tryptophan residues as the fluorophore showed binding of hVN1R1 to its ligand myrtenal, giving an EC_{50} of approximately 1 μM [81]. In three similar studies, MST was used to measure binding of human and mouse olfactory receptors and GPCRs solubilised with designer lipid-like peptides to their respective ligands. Here native tryptophan residues in the receptors were used as the fluorescence source for MST, and measured EC_{50} values ranged from 0.9 to 86 μM [82-84]. In a study reporting the cell-free expression, purification and ligand-binding analysis of olfactory receptors DmOR67a, DmOR85b and DmORCO from *Drosophila melanogaster*, MST was used to demonstrate that they bind their respective ligands. DmOR67a and DmORCO were titrated individually and together with ethyl benzoate, while DmOR85b and DmORCO were titrated individually and together with 2-heptanone. When DmOR67a was co-incubated with DmORCO, ethyl benzoate bound with an affinity of ~0.5 ± 0.1 μM, and when DmOR85b was co-incubated with DmORCO, 2-heptanone bound with an affinity of ~0.8 ± 0.2 μM [85].

In a study that computationally designed and characterised nanobody-derived peptides (NDPs) to stabilise the active conformation of the human β2-adrenergic receptor (β2-AR), MST measured binding of a selected 17-residue NDP (P3) to the β2-AR. The agonist(isoproterenol)-activated β2-AR displayed a ~10-fold higher affinity for P3 than the unstimulated receptor, with EC_{50} values of 3.57 μM and 58.22 μM, respectively [86]. MST was used to observe binding of the peptide neurotransmitter neurotensin (NT) to the human dopamine receptor 1 (D1) under native conditions in polymer-assembled Lipodisqs (Fig. 3). The Lipodisqs were formed by adding the copolymer styrene-maleic acid (SMA) to membranes expressing D1 at a membrane:SMA w/w ratio of 1:1.5. MST measurements used Cy5-labelled NT, which had an estimated binding affinity for D1 Lipodisqs of >300 nM [87]. An MST method was developed to measure ligand/receptor binding in non-purified samples of the dopamine D2 receptor (D2R). The concentration of D2R in mammalian cell plasma membranes from induced HekD2 cells was determined to be 36.8 ± 2.6 pmol/mg. Dose-response curves determined the binding affinity (K_D) for the fluorescent ligand spiperone—Cy5 to be 5.3 ± 1.7 nM. To eliminate the possibility of non-specific binding between spiperone—Cy5 and the cell membranes, the measurements were performed both in the absence and in the presence of the D2R antagonist haloperidol [88].

In a study demonstrating that down-regulation of the endothelial protein C receptor (EPCR) promotes preeclampsia by affecting actin polymerization, MST was used to observe direct binding of EPCR to protease-activated receptor 1 (PAR-1), which is a GPCR [89]. A plethora of techniques were used to identify macrophage migration inhibitory factor (MIF) as an atypical chemokine (ACK) that binds to chemokine receptors CXCR2 and CXCR4 to promote atherogenic leukocyte recruitment. This included use of MST to confirm the interaction between MST-Red-labelled MIF and platelet chemokine CXCL4L1. Titration of MST-Red-MIF with increasing concentrations of CXCL4L1 produced a binding constant (K_D = 159.8 ± 16.8 nM) that was similar to that obtained by SPR (K_D = 116 ± 16 nM) [90].

6.3 Other Receptors

Various other receptors have been analysed by MST, including measurement of metallothionein binding to the lipocalin-2 (24p3/neutrophil gelatinase-associated lipocalin (NGAL)) receptor (SLC22A17) in CHO plasma membrane vesicles, giving an EC_{50} of 123 ± 50 nM [91]. MST was used to characterise interactions between the membrane-bound mucin MUC4 and the ErbB2 receptor, which occurs at the cancer cell surface. Lysates of CHO cells were used that contained the transmembrane β subunit of MUC4 (MUC4β) or a mutant containing only the EGF domains (MUC4EGF3+1+2). K_D values for binding of ErbB2 to MUC4β-ErbB2 and MUC4EGF3+1+2 were measured at 7-25 nM and 65-79 nM, respectively [92].

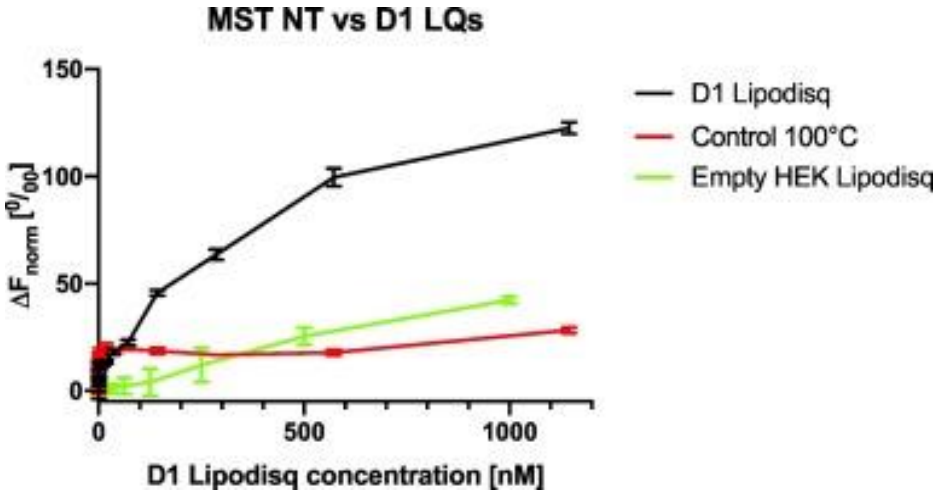

Fig. 3. Binding of neurotensin (NT) to the human dopamine receptor 1 (D1) in polymer-assembled Lipodisqs

MST used Cy5-labelled NT (NT-Cy5). The affinity of NT-Cy5 for D1 Lipodisqs was >300 nM. Denatured D1 Lipodisqs and Lipodisqs formed from HEK cells lacking D1 (red and green curves, respectively) did not show binding to NT. Error bars represent the standard error of n = 3 measurements. This figure was reproduced from Bada Juarez et al. (2020) [87]

MST was used to analyse ligand-specific conformational states of the human glycine receptor (GlyR), which is a member of the pentameric ligand-gated ion channel (pLGIC) family. The fluorescent-labelled GlyR alpha-1 subunit was solubilised in amphipathic styrene-maleic acid copolymer nanodiscs. MST measurements showed that the full agonist glycine and the partial agonist taurine induced different conformational transitions on binding to the GlyR, giving EC_{50} values of 65 ± 22.8 µM and 473.8 ± 66.1 µM, respectively (Figure 4). The results indicated that partial agonism in pLGIC proteins is reflected by the adaption of distinct receptor conformations [93].

MST was used to measure binding of FIP-nha (a fungal immunomodulatory protein from *Nectria haematococca*) to the labelled human epidermal growth factor receptor EGFR (K_D = 15.54 ± 2.93 µM) [94]. In a study that performed in silico screening of the binding affinities of fifty curcumin derivatives to the human EGFR by a molecular docking approach, MST was used to validate the results. The predicted EGFR-ligand binding constants were in the range of 0.00013 ± 0.00006 to 3.45 ± 0.10 µM. MST measured binding constants for curcumin (K_D = 5.1 ± 0.33 µM), N-(3-nitrophenylpyrazole) curcumin (K_D = 19.7 ± 2.1 µM), and derivative 1A9 (K_D = 4.9 ± 0.62 µM) [95].

A study demonstrated how the chemotherapeutic agent cisplatin interacts with toll-like receptor 4 (TLR4) to initiate proinflammatory signalling that underlies cisplatin toxicities. Soluble TLR4 blocked cisplatin-induced, but not lipopolysaccharide-induced, TLR4 activation. In MST experiments nickel and cisplatin, but not lipopolysaccharide, showed direct binding to human TLR4 with K_D values of 2.72 µM and 50.57 µM, respectively. Mouse TLR4 showed binding to cisplatin (K_D = 104.9 µM) but not to nickel [96].

MST was used to measure binding of lipoprotein ligands to two human class B scavenger receptors, scavenger receptor class B type 1 (SR-B1) and CD36, which are receptors for high-density lipoproteins and oxidized low-density lipoproteins, respectively. Using receptors labelled with Cy5 at lysine residues, SR-B1 bound to lipid-free apolipoprotein A-I with a K_D of 82 ± 12 µg/ml or 2.73 ± 0.40 µM and to holoparticle high-density lipoprotein (HDL) with a K_D of 52 ± 9 µg/ml or 194 ± 34 nM. CD36 bound oxidized low-density lipoprotein (oxLDL) with a K_D of 1.2 ± 0.5 mg/ml or 342.86 ± 285.71 nM and bound human HDL with a K_D of 33 ± 8 µg/ml or 123.36 ± 29.9 nM. There was no difference in affinity of SR-B1 for HDL or CD36 for oxLDL when comparing glycosylated and deglycosylated receptors [97].

MST was also used to measure binding of Staphylococcus enterotoxin B (SEB) to the human natural killer cell receptor 2B4 (CD244) [98].

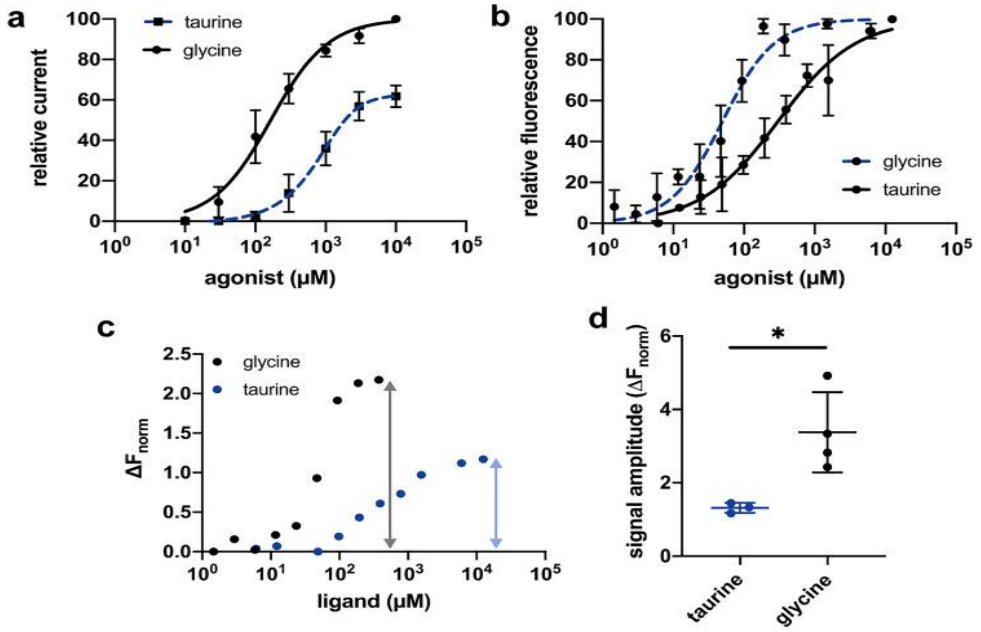

Fig. 4. Binding characteristics of the partial agonist taurine to α1-GFP GlyR nanodiscs

(*a) Dose–response data for glycine and taurine of heterologous expressed α1 GlyR from Xenopus laevis oocytes. Taurine acts as a partial agonist with an a EC_{50} value of 843 ± 16 μM reaching a maximum current of 61% compared to glycine (n = 3). Taurine currents are normalized to the maximum glycine currents for each cell. Error bars represent SEM. (b) MST binding experiment of α1-GFP GlyR with a taurine titration series of 6 μM to 12.5 mM results in a cEC_{50} value of 473.8 ± 46.1 μM (n = 3). Error bars represent SEM. (c) Exemplary α1-GFP GlyR MST data of taurine (blue circles) and glycine (black circles) obtained from oocytes displaying a difference in their maximal thermophoretic mobility (grey and blue arrows). (d) Comparison of the signal amplitudes of α1-GFP GlyR SMALPs expressed in HEK293 cells and oocytes for glycine and taurine. Binding of taurine leads to a significantly decreased thermophoretic movement (p = 0.024, unpaired two-side t test, n = 3) with signal amplitudes of 1.32 ± 0.14 compared to glycine-bound receptors with signal amplitudes of 3.38 ± 1.09. Data are shown in mean ± SD. This figure was reproduced from Bernhard and Laube (2020) [93]*

6.4 Sensor Kinases

MST has been used to analyse some histidine and tyrosine kinases. In a study that investigated interactions in the Cpx two component system of *E. coli*, MST was used to measure binding affinities between the sensor histidine kinase CpxA with its cognate response regulator CpxR and its accessory protein CpxP. CpxA was reconstituted in MSP1D1 nanodiscs and MST measurements used fluorescently-labelled CpxA-Strep or MSP1D1. CpxA had a high affinity for CpxR (K_D = 3.7 ± 0.5 μM), which was increased by around 10-fold by phosphorylation (K_D = 0.55 ± 0.06 μM). The affinity between CpxA and CpxP was much lower (K_D >100 μM) [99].

A range of biophysical techniques and cell-based assays were used to identify a highly selective small molecule inhibitor of lemur tyrosine kinase 3 (LMTK3), which is a dual specificity serine/threonine kinase with an oncogenic role in various tumour types and a viable therapeutic target. The analyses included use of MST to obtain binding curves for the new inhibitor C36 (K_D = 1.87 ± 0.2 μM) and an existing inhibitor C28 (K_D = 2.50 ± 0.4 μM) with human LMTK3 [100].

6.5 Ion Channels

Several studies have used MST to analyse interactions with the voltage-dependent anion channel 1 (VDAC1). In a study that looked at mediation of the antiapoptotic activity of Bcl-xL protein upon interaction with mouse VDAC1, MST was used to observe binding of fluorescently labelled Bcl-xL to VDAC1, giving a binding affinity of 0.67 μM [101]. In a study that demonstrated direct modulation of human VDAC1 by cannabidiol (CBD), MST was used to show a direct interaction between purified fluorescently labelled VDAC1 and CBD, giving a K_D of 11.2 ± 6 μM [102]. In a study that demonstrated how VDAC1 mediates amyloid β (Aβ) toxicity and is a potential target for

Alzheimer's disease therapy, MST was used to observe Aβ binding to fluorescently-labelled human VDAC1 with a K_D of 50 µm. In an MST experiment using intrinsic VDAC1 tryptophan fluorescence, Aβ binding resulted in a K_D of 16.6 µM [103]. Seventeen small-molecule compounds were screened for interaction with human mitochondrial VDAC1 using nano-differential scanning fluorimetry and MST (Figure 5). The dissociation constants for fifteen of the compounds were measured by MST with six successfully determined: DIDS (K_D = 0.5 µM), VBIT4 (K_D = 3 µM), itraconazole (K_D = 5 µM), cannabidiol (K_D = 6 µM), curcumin (K_D = 6 µM), emodin (K_D = 10 µM). It was noted that DIDS is likely to interact covalently with VDAC1, which should be considered in evaluating the measured K_D. Four of the compounds (cannabidiol, curcumin, DIDS and VBIT4) were identified as potential starting points for future design of VDAC1 selective ligands [104]. In a study that demonstrated how a cholesterol analogue induces an oligomeric reorganization of VDAC, MST was used to measure binding of hexokinase isoform I (HK-I) to VDAC from *Neurospora crassa*, giving a binding constant of 27 ± 6 µM in the presence of cholesteryl-hemisuccinate. There was no binding of hexokinase isoform II (HK-II) [105].

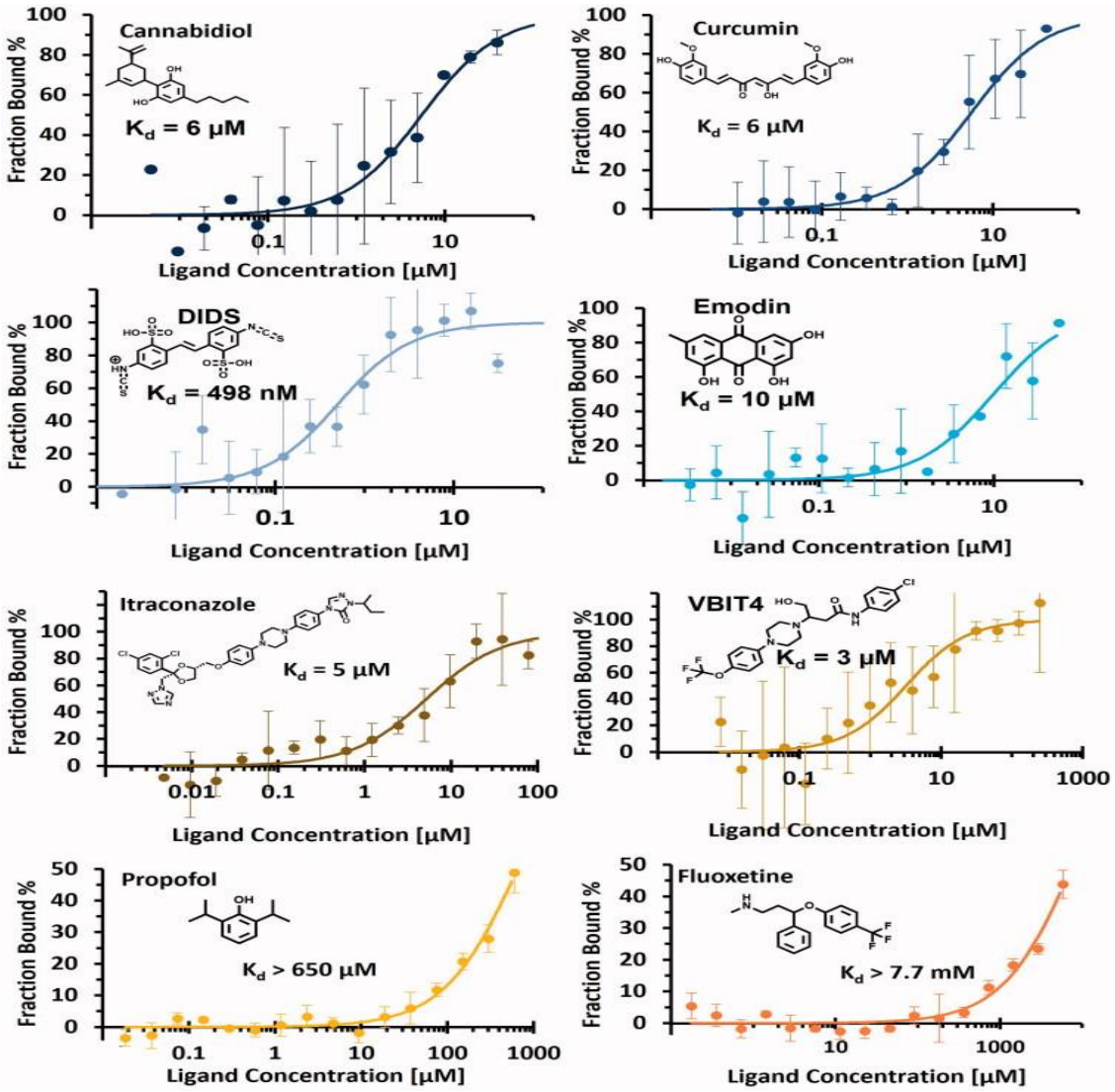

Fig. 5. MST dose-response curves of eight compounds with human mitochondrial VDAC1.
Precise or minimum K_D values are displayed for cannabidiol, curcumin, DIDS, emodin, itraconazole, VBIT4, propofol and fluoxetine. Error bars show standard deviation obtained from three replicas of the same measurement. This figure was reproduced from Gorny et al. [104]

In a study of competitive interactions between the phosphoinositide regulator of TRP (PIRT), the cold sensing ion channel TRPM8, and the signalling phosphoinositide lipid PIP2, MST was used identify a competitive PIRT interaction between PIP2 and the TRPM8 S1-S4 transmembrane domain [106].

MST measured binding of the tarantula gating-modifier toxins ProTx-II and GpTx-I to the voltage sensing domain (VSD) of repeat II of the human voltage-gated sodium channel NaV1.7 [107]. Residues 732-860, which contain three transmembrane helices, were recombinantly expressed, purified and reconstituted in DMPC lipids. For MST, VSD2 in DMPC was titrated into 50 nM toxins fluorescently labelled with Alexa Fluor™ 488. Binding affinities (K_D values) for ProTx-II and GpTx-I were measured at 200 nM (160-250 nM) and 700 nM (300-1500), respectively. In comparison, IC_50 values for ProTx-II inhibition of full-length NaV1.7 in membranes had been reported in the range 0.3-3 nM. Mutations F813A and D816A in VSD2 increased the K_D values for GpTx-I binding to 300 nM (600-3000) and 5000 nM (3000-15,000 nM), respectively [107].

In a study that demonstrated how chloride intracellular channel 1 (CLIC1) activity is not required for glioblastoma development, but its inhibition dictates glioma stem cell responsivity to novel biguanide derivatives, MST was used to measure the interaction of two biguanide compounds (Q48 and Q54) with recombinant CLIC1 protein. CLIC1 was labelled with red and blue dye kits and dose-response curves measured binding affinities of $K_D = 15.6 \pm 1.9$ µM and $K_D = 1.9 \pm 0.5$ mM for Q48 and Q54, respectively [108].

MST was used to measure direct interactions between phosphoinositides and potassium channel KcsA. Using a range of phospholipids it was found that there was a general increase in binding affinity with the number of negative charges. The phosphoinositides PI(4)P (phosphatidylinositol 4-phosphate), PI(3,4)P2 (phosphatidylinositol 3,4-bisphosphate), PI(4,5)P2 (phosphatidylinositol 4,5-bisphosphate), PI(3,4,5)P3 (phosphatidylinositol 3,4,5-trisphosphate) with two to four net negative charges produced greater binding effects than POPC (1-palmitoyl-2-oleoylphosphatidylcholine) with no charge, and POPG (1-palmitoyl-2-oleoylphosphatidylglycerol) and PI (phosphatidylinositol) with one net negative charge [109].

MST was also used to measure the direct interaction between the purified voltage-gated proton channel (Hv1) from mouse and ATP [110].

6.6 Aquaporins

MST has been used to measure interactions with some aquaporins. In a study that demonstrated how phosphorylation of human aquaporin 2 (AQP2) allosterically controls its interaction with the lysosomal trafficking regulator-interacting protein LIP5, MST was used to measure binding of fluorescently-labelled LIP5 to wild-type and mutant forms of AQP2. Non-phosphorylated wild-type AQP2 bound LIP5 with the highest affinity ($K_D = 191 \pm 43.2$ nM), whilst AQP2-ΔP242 had 20-fold lower affinity ($K_D = 3.63 \pm 0.44$ µM). AQP2-S256E ($K_D = 1.00 \pm 0.25$ µM), S261E ($K_D = 745 \pm 141$ nM), T269E ($K_D = 721 \pm 55.0$ nM), and S256E/T269E ($K_D = 652.7 \pm 62.2$ nM) all had reduced affinity. AQP2-S264E had an affinity similar to non-phosphorylated wild-type AQP2 ($K_D = 278 \pm 49.1$ nM) [111]. More recently, a protocol was developed for characterizing the binding between a human aquaporin and a soluble interaction partner using MST [112], and MST was used to measure the interaction of *Zea mays* aquaporin ZmPIP2;5 with the jasmonic acid analogue coronatine [113].

6.7 Transporters

Interactions with a variety of transport proteins have been analysed by MST, including binding of purine and pyrimidine nucleosides to equilibrative nucleoside transporter 7 (ENT7) from *Arabidopsis thaliana* fused with eGFP [114]. An MST ligand-binding assay for characterising solute carriers was demonstrated using the SLC15 oligopeptide transporter PepT1. An SLC15A1/PepT1 ortholog from the moss *Physcomitrella patens* (PepTPp), which is highly similar to human PepT1, was expressed in yeast. The method compared the analysis of solubilised total membrane preparations with or without expression of PepTPp, using a yeast strain (*Saccharomyces cerevisiae*), in which the corresponding endogenous SLC homolog is depleted and using the dipeptide glycylsarcosine (Gly-Sar) and the antiviral prodrug valacyclovir as test ligands. Gly-Sar was bound in the mM range and valacyclovir had a K_D of around 50 µM [115].

In a study that dissected the protonation sites for antibacterial recognition and transport in the multidrug efflux transporter QacA from *Staphylococcus aureus*, MST was used to measure binding of substrates to purified wild-type and mutant forms of QacA. Wild-type QacA had K_D values for binding tetraphenylphosphonium, pentamidine and dequalinium of 0.36 ± 0.07 mM, 1 ± 0.17 mM and 0.90 ± 0.21 mM, respectively [116].

In a study that identified a grafted hyaluronic acid N-acetyl-l-methionine (HA-ADH-AcMet) to target the human L-type amino acid transporter-1 (LAT1), MST was used to measure the binding affinity of different ligands to LAT1. The highest affinity ligand was HA-ADH-AcMet with a K_D of 408 nM [117].

In a study investigating functional sites in the Major Facilitator Superfamily (MFS) efflux protein NorA from *Staphylococcus aureus*, MST was used to measure the binding of tetraphenylphosphonium chloride to GFP-fused wild-type and mutant NorA. GFP was fused between residues 153 and 154 of NorA, flanked by a peptide 'GGSGG'. Tetraphenylphosphonium chloride binding to GFP-NorA and a multisite mutation (F16A/E222A/F303A/D307A) of GFP-NorA had K_D values of 7.6 ± 2 mM and 16.7 ± 6 mM, respectively [118].

Along with other techniques, MST was used in a study of the structural basis for arsenite binding and translocation of the Acr3 antiporter from *Bacillus subtilis* [119]. Acr3 is an efflux pump that confers resistance to arsenite, it has nine transmembrane helices that display a typical NhaA structure fold, with two discontinuous helices of transmembrane segments (TM4 and TM9) interacting with each other and forming an X-shaped structure. MST measured arsenite binding to GFP-labelled wild-type Acr3 and individual mutants of Acr3 (R118A, N144A, E295A, E322A) to give K_D values of 2.9, 14.8, 11.9,19.6 and 27.5 mM, respectively (Figure 6). The study identified motif C in TM9 to be critical for substrate binding, in which N292 and E295 are involved in substrate coordination, while R118 in TM4 and E322 in TM10 are responsible for structural stabilization. Highly conserved residues on motif B in TM5 were found to be important in the protonation/deprotonation process [119].

A comprehensive study on the energy coupling and stoichiometry of Zn^{2+}/H^+ antiport by the cation diffusion facilitator YiiP from *Shewanella oneidensis* used MST to assess the binding affinity of individual Zn^{2+} binding sites and to explore the basis for coupling of Zn^{2+} transport to the proton-motive force [120]. YiiP functions as a homodimer and has three distinct Zn^{2+} binding sites referred to as A, B and C. Site A is in the transmembrane domain and has three Asp and one His residue where it is alternately exposed to the cytoplasm or to the periplasm in inward- and outward-facing states, respectively. Site B is on the loop between transmembrane helices 2 and 3 and has two His and one Asp residue. Site C is in the C-terminal domain and is a binuclear site (C1 and C2) with four His and two Asp residues. For assessing Zn^{2+} binding to individual Zn^{2+} binding sites a series of mutants was used to isolate the individual sites. The triple mutant D70A/D287A/H263A was used to study site A, D51A/D287A/H263A was used to study site B, and D51A/D70A was used to study site C. At pH 7, MST measured relatively high affinity for sites A and C with K_D values of 16 nM and 33 nM, respectively, and lower affinity for site B with a K_D value of 1.2 µM. When further mutations were introduced to isolate the individual C1 (D51A/D70A/H263A) and C2 (D51A/D70A/H234A) sites, the binding affinity was reduced to give K_D values of 153 nM and 223 nM, respectively, suggesting cooperative binding of Zn^{2+} at C1 and C2 [120]. The basis for coupling of Zn^{2+} transport to the proton-motive force was investigated by measuring Zn^{2+} binding affinities at pH values of 5.6 to 7.4.

6.8 Other Membrane Proteins

In a study that investigated unwinding of the substrate transmembrane helix in intramembrane proteolysis, MST measured binding of a chimeric substrate MBP-Gurken-TMD to wild-type and mutant forms of the intramembrane-cleaving proteases (I-CLiPs) rhomboid protease GlpG from *E. coli* and MCMJR1 from archaea. GlpG and MCMJR1 were labelled with fluorescent dye NT-647. MBP-Gurken-TMD bound to wild-type and a mutant (H254A) of GlpG in 0.1% DDM with K_D values of ~1.4 µM and ~0.7 µM, respectively (Figure 7). Binding did not reach saturation because a higher concentration of substrate could not be achieved due to aggregation. MBP-Gurken-TMD bound to MCMJR1 in 0.1% DDM with a K_D of ~9 µM [121].

In a study that demonstrated how lysosomal integral membrane protein-2 (LIMP-2/SCARB2) is involved in lysosomal cholesterol export, MST

was used to detect a direct interaction between fluorescently labelled human LIMP-2 and cholesterol, giving an EC_{50} of 112 ± 32 nM [122]. In a study that demonstrated how human tetraspanin CD82 interacts with cholesterol to promote extracellular vesicle-mediated release of ezrin to inhibit tumour cell movement, MST was used to determine the cholesterol-binding affinity of CD82. MST was performed on GFP-labelled wild-type and LYK mutant CD82 proteins expressed at similar levels in Du145 cells. Cholesterol bound to CD82-wild-type with a K_D of 5.89 µM but did not bind to CD82-LYK [123].

MST was used to show how the human phosphoinositide-interacting regulator of TRP (PIRT) binds calmodulin and cholesterol-like ligands. PIRT had high affinity for calcium-free calmodulin (apo-CaM) and lower affinity for calcium bound calmodulin, with K_D values of 350 ± 40 nM and 60 ± 30 µM, respectively. Cholesteryl-hemisuccinate had a K_D of 103 ± 6 µM, and cortisol and β-estradiol had K_D values of 790 ± 60 µM and 800 ± 100 µM, respectively. Despite the structural similarity of testosterone to cholesterol, cortisol and β-estradiol, it did not show binding to PIRT [124].

Occludin is a tetramembrane-spanning tight junction protein, which possesses a bundle of three α-helices that mediates interactions with other tight junction components. A study demonstrated that serine 408 phosphorylation is a molecular switch that regulates structure and function of occludin, where a short unstructured region next to the α-helical bundle is a hotspot for phosphorylation. Here NMR was used to define the effects of S408 phosphorylation on intramolecular interactions between the unstructured region and the α-helical bundle, then paramagnetic relaxation enhancement and MST were used to demonstrate that the unstructured region interacts with the α-helical bundle, and binding was enhanced by S408 phosphorylation [125].

MST with nanodiscs was used to confirm the micromolar affinity of perforin for calcium ions, which is required for perforin interaction with the membrane. MSP nanodiscs containing 1-palmitoyl-2-oleoyl-sn-glycero-3-phosphocholine (POPC) and 1,2-dioleoyl-sn-glycero-3-phosphoethanolamine (DOPE) labelled with fluorescent dye Atto-647 (DOPEAtto-647) were used to reconstitute human and mouse perforin, giving K_D values of 123 ± 33 µM and 26 ± 5.8 µM, respectively [126].

Using multiple biophysical techniques, it was demonstrated that human mitochondrial fission protein 1 (Fis1) directly interacts with dynamin related protein 1 (Drp1) in an evolutionarily conserved manner to promote mitochondrial fission. For MST experiments, Fis1 with its N-terminal arm removed (Fis1ΔN9-125) and Drp1 were covalently modified at methionine residues with a Cy5-azide fluorophore. Propargyl oxaziridine was used to generate a sulfimide conjugate to methionine containing a terminal alkyne, then copper click chemistry was used to attach Cy5. In MST experiments monitoring Cys5-Drp1 fluorescence, 30 µM Drp1 was titrated with Fis1ΔN to give an apparent affinity (app K_D) of Drp1 for Fis1ΔN of 12 ± 2 µM (Figure 8) [127].

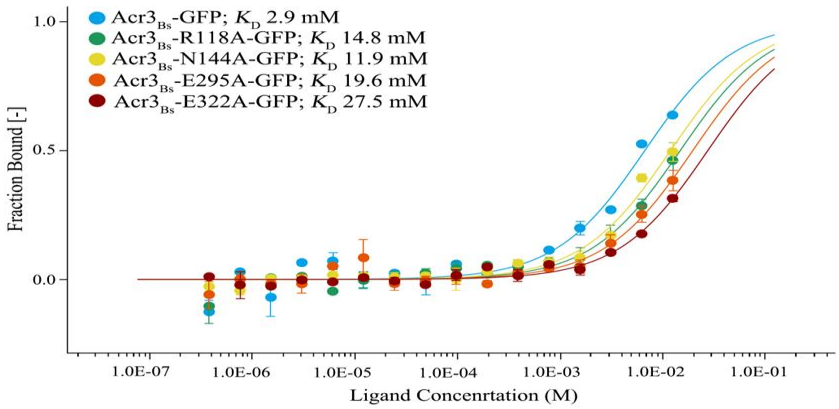

Fig. 6. MST analysis of arsenite binding to GFP-labelled wild-type and mutant forms of the Acr3 antiporter from *Bacillus subtilis*

Affinity analysis with a K_D model and fitted by fraction bound normalisation. Experiments were conducted in triplicate. This figure was reproduced from Lv et al. [119]

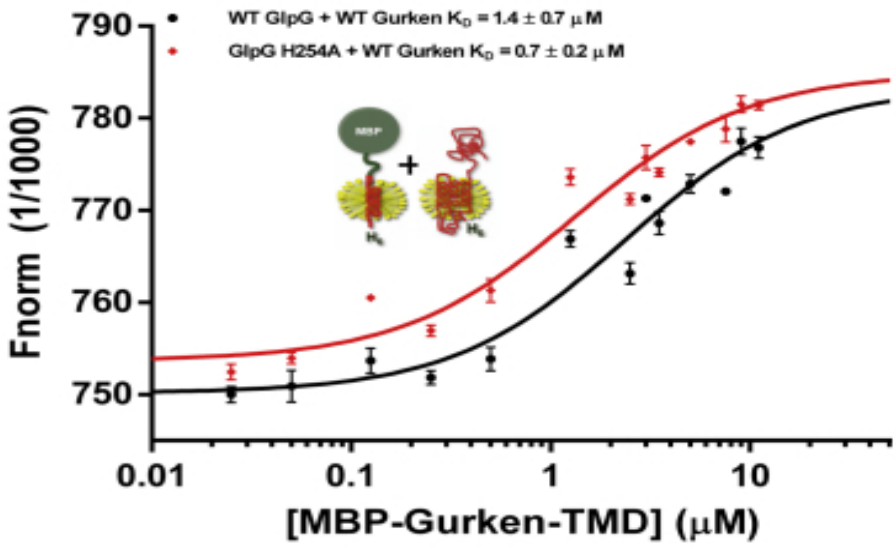

Fig. 7. MST binding curves of the P252A MBP-Gurken-TMD variant to wild-type GlpG and the inactive H254A GlpG variant in 0.1% DDM

This figure was reproduced from Brown et al. [121]

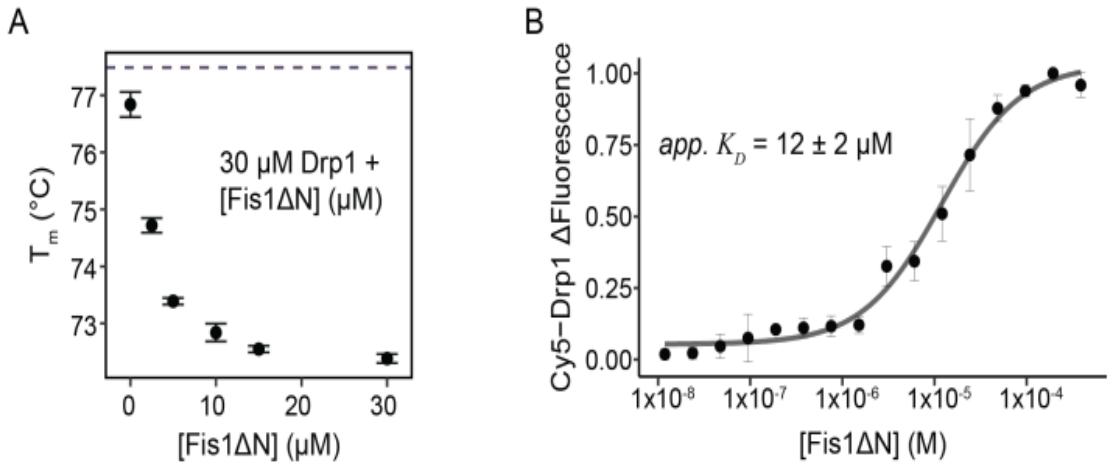

Fig. 8. Removal of the Fis1 N-terminal arm reveals Drp1 binding and prevents Drp1 assembly *in vitro*

***A**. Box plot depicting the global unfolding temperature (T_m) of 30 μM Drp1 in the presence of increasing Fis1ΔN (0-30 μM). T_m values determined as the temperature corresponding to the first derivative of the maximum fluorescence value. N=2 for each titration point. B. ΔFluorescence values of 80 nM Cy5-Drp1 in the presence of increasing Fis1ΔN as determined by MST and fit to a single-site binding model to determine an apparent K_D value. ΔFluorescence values normalized to a 0-1 scale to allow for comparisons and averaging between multiple experiments (n=3), error bars=SD. This figure was reproduced from Nolden et al. [127]*

7. CONCLUSION

In reviewing the analysis of membrane proteins by MST we have consolidated the opinion that MST is a useful technique for studying biomolecular interactions with membrane proteins. This is because MST has no limitations on the size of the target biomolecule, on the affinity of the interaction being studied or on the composition of the buffer and other sample components, and it uses much less sample compared to other techniques that measure biomolecular interactions. Different types of membrane proteins from different organisms have been studied by MST with the protein in cell lysates or native membranes, solubilised in

detergents, or reconstituted in lipids, nanodiscs or Lipodisqs. Very few of these studies used intrinsic aromatic residues as the fluorophore for MST measurements. The large majority of studies used proteins labelled with different fluorescent dyes or conjugated with GFP. It is important that the sample conditions and the labelling strategy being used for MST measurements do not adversely affect the native structure and activity of the protein. The best studies are therefore those that use other biophysical and biochemical techniques alongside MST to test the structural integrity and activity of the membrane protein under the same conditions as those used for MST. The many interactions that MST can measure with membrane proteins include those with other proteins and peptides, nucleic acids, detergents and lipids, liposomes and vesicles, or small molecules and ions. MST is therefore a useful technique to have in drug screening projects with membrane protein targets.

COMPETING INTERESTS

Authors have declared that no competing interests exist.

REFERENCES

1. Wienken CJ, Baaske P, Rothbauer U, Braun D, Duhr S. Protein-binding assays in biological liquids using microscale thermophoresis. Nat Commun. 2010;1: 100.
2. Jerabek-Willemsen M, Wienken CJ, Braun D, Baaske P, Duhr S. Molecular interaction studies using microscale thermophoresis. Assay Drug Dev Technol. 2011;9(4):342-353.
3. Seidel SA, Dijkman PM, Lea WA, van den Bogaart G, Jerabek-Willemsen M, Lazic A et al. Microscale thermophoresis quantifies biomolecular interactions under previously challenging conditions. Methods. 2013;59 (3):301-315.
4. Alexander CG, Wanner R, Johnson CM, Breitsprecher D, Winter G, Duhr S et al. Novel microscale approaches for easy, rapid determination of protein stability in academic and commercial settings. Biochim Biophys Acta. 2014;1844(12): 2241-2250.
5. Jerabek-Willemsen M, André T, Wanner R, Roth RM, Duhr S, Baaske P, Breitsprecher D. Microscale thermophoresis: Interaction analysis and beyond. J Mol Struct. 2014;1077:101-113.
6. Mao Y, Yu L, Yang R, Qu LB, Harrington Pde B. A novel method for the study of molecular interaction by using microscale thermophoresis. Talanta. 2015;132:894-901.
7. Linke P, Amaning K, Maschberger M, Vallee F, Steier V, Baaske P, Duhr S, Breitsprecher D, Rak A. An automated microscale thermophoresis screening approach for fragment-based lead discovery. J Biomol Screen. 2016;21(4):41 4-421.
8. Rainard JM, Pandarakalam GC, McElroy SP. Using microscale thermophoresis to characterize hits from high-throughput screening: A European lead factory perspective. SLAS Discov. 2018;23(3):2 25-241.
9. Holdgate G, Embrey K, Milbradt A, Davies G. Biophysical methods in early drug discovery. ADMET DMPK. 2019;7(4):222-241.
10. Mrozowich T, Meier-Stephenson V, Patel TR. Microscale thermophoresis: warming up to a new biomolecular interaction technique. Biochem (Lond). 2019;41(2):8-12.
11. El Deeb S, Al-Harrasi A, Khan A, Al-Broumi M, Al-Thani G, Alomairi M et al. Microscale thermophoresis as a powerful growing analytical technique for the investigation of biomolecular interaction and the determination of binding parameters. Methods Appl Fluoresc. 2022; 10(4).
DOI: 10.1088/2050-6120/ac82a6
12. Magnez R, Bailly C, Thuru X. Microscale thermophoresis as a tool to study protein interactions and their implication in human diseases. Int J Mol Sci. 2022;23(14):7672.
13. Sparks RP, Lawless W, Arango AS, Tajkhorshid E, Fratti RA. Use of microscale thermophoresis to measure protein-lipid interactions. J Vis Exp. 2022;180:e60607.
14. Asmari M, Michalcová L, Ibrahim AE, Glatz Z, Wätzig H, El Deeb S. Studying molecular interactions via capillary electrophoresis and microscale thermophoresis: A review. Electrophoresis. 2023;44(13-14):1114-1142.
15. Scheuermann TH, Padrick SB, Gardner KH, Brautigam CA. On the acquisition and analysis of microscale thermophoresis data. Anal Biochem. 2016;496:79-93.

16. Stein JAC, Ianeselli A, Braun D. Kinetic Microscale thermophoresis for simultaneous measurement of binding affinity and kinetics. Angew Chem Int Ed Engl. 2021;60(25):13988-13995.
17. Tso SC, Brautigam CA. Measuring the KD of protein-ligand interactions using microscale thermophoresis. Methods Mol Biol. 2021;2263:161-181.
18. Huang Y, Li Y. Microscale thermophoresis assay: A powerful method to quantify protein-nucleic acid and protein-protein interactions. Methods Mol Biol. 2022;2400:21-31.
19. Maynard JA, Lindquist NC, Sutherland JN, Lesuffleur A, Warrington AE, Rodriguez M, Oh SH. Surface plasmon resonance for high-throughput ligand screening of membrane-bound proteins. Biotechnol J. 2009;4(11):1542-1558.
20. Locatelli-Hoops S, Yeliseev AA, Gawrisch K, Gorshkova I. Surface plasmon resonance applied to G protein-coupled receptors. Biomed Spectrosc Imaging. 2013;2(3):155-181.
21. Livnat Levanon N, Vigonsky E, Lewinson O. Real time measurements of membrane protein:receptor interactions using Surface Plasmon Resonance (SPR). J Vis Exp. 2014;(93):e51937.
22. Patching SG. Surface plasmon resonance spectroscopy for characterisation of membrane protein-ligand interactions and its potential for drug discovery. Biochim Biophys Acta – Biomembranes. 2014;183 8(1 Pt A):43-55.
23. Shepherd C, Robinson S, Berizzi A, Thompson LEJ, Bird L, Culurgioni S, Varzandeh S, Rawlins PB, Olsen RHJ, Navratilova IH. Surface plasmon resonance screening to identify active and selective adenosine receptor binding fragments. ACS Med Chem Lett. 2022;13 (7):1172-1181.
24. Draczkowski P, Matosiuk D, Jozwiak K. Isothermal titration calorimetry in membrane protein research. J Pharm Biomed Anal. 2014;87:313-25.
25. Rajarathnam K, Rösgen J. Isothermal titration calorimetry of membrane proteins - progress and challenges. Biochim Biophys Acta. 2014;1838(1 Pt A):69-77.
26. Situ AJ, Schmidt T, Mazumder P, Ulmer TS. Characterization of membrane protein interactions by isothermal titration calorimetry. J Mol Biol. 2014;426(21):3670-3680.
27. Boudker O, Oh S. Isothermal titration calorimetry of ion-coupled membrane transporters. Methods. 2015;76:171-182.
28. Liu S, Lockless SW. Ion binding to transport proteins using isothermal titration calorimetry. Methods Mol Biol. 2018;1684:289-303.
29. Lin K, Wu G. Isothermal titration calorimetry assays to measure binding affinities in vitro. Methods Mol Biol. 2019;1893:257-272.
30. Vu HN, Situ AJ, Ulmer TS. Isothermal titration calorimetry of membrane proteins. Methods Mol Biol. 2021; 2302: 69-79.
31. Deshayes S, Divita G. Fluorescence technologies for monitoring interactions between biological molecules in vitro. Prog Mol Biol Transl Sci. 2013;113:109-143.
32. Niebling S, Burastero O, García-Alai M. Biophysical characterization of membrane proteins. Methods Mol Biol. 2023; 2652:215-230.
33. Siligardi G, Hussain R, Patching SG, Phillips-Jones MK. Ligand- and drug-binding studies of membrane proteins revealed through circular dichroism spectroscopy. Biochim Biophys Acta – Biomembranes. 2014;1838(1 Pt A):34-42.
34. Miles AJ, Wallace BA. Circular dichroism spectroscopy of membrane proteins. Chem Soc Rev. 2016;45(18):4859-4872.
35. Hussain R, Siligardi G. Characterisation of conformational and ligand binding properties of membrane proteins using synchrotron radiation circular dichroism (SRCD). Adv Exp Med Biol. 2016;922:43-59.
36. Patching SG. Spermidine binding to the *Acetinobacter baumannii* efflux protein AceI observed by near-UV synchrotron radiation circular dichroism spectroscopy. Radiation. 2022;2(2):228-233.
37. Lakatos A, Mörs K, Glaubitz C. How to investigate interactions between membrane proteins and ligands by solid-state NMR. Methods Mol Biol. 2012;914:65-86.
38. Ghitti M, Musco G, Spitaleri A. NMR and computational methods in the structural and dynamic characterization of ligand-receptor interactions. Adv Exp Med Biol. 2014;805:271-304.
39. Oxenoid K, Chou JJ. A functional NMR for membrane proteins: dynamics, ligand binding, and allosteric modulation. Protein Sci. 2016;25(5):959-973.

40. Patching SG. NMR-active nuclei for biological and biomedical applications. Journal of Diagnostic Imaging in Therapy. 2016;3(1):7-48.
41. Bondarenko V, Wells M, Xu Y, Tang P. Solution NMR studies of anesthetic interactions with ion channels. Methods Enzymol. 2018;603:49-66.
42. Dikiy I, Clark LD, Gardner KH, Rosenbaum DM. Isotopic labeling of eukaryotic membrane proteins for NMR studies of interactions and dynamics. Methods Enzymol. 2019;614:37-65.
43. Puthenveetil R, Vinogradova O. Solution NMR: A powerful tool for structural and functional studies of membrane proteins in reconstituted environments. J Biol Chem. 2019;294(44):15914-15931.
44. Raingeval C, Krimm I. NMR investigation of protein-ligand interactions for G-protein coupled receptors. Future Med Chem. 2019;11(14):1811-1825.
45. Danmaliki GI, Hwang PM. Solution NMR spectroscopy of membrane proteins. Biochim Biophys Acta Biomembr. 2020;6 2(9):183356.
46. Yeh V, Goode A, Bonev BB. Membrane protein structure determination and characterisation by solution and solid-state NMR. Biology (Basel). 2020;9(11):396.
47. Almeida TB, Panova S, Walser R. NMR reporter assays for the quantification of weak-affinity receptor-ligand interactions. SLAS Discov. 2021;26(8):1020-1028.
48. Höfurthner T, Mateos B, Konrat R. On-cell NMR contributions to membrane receptor binding characterization. Chempluschem. 2021;86(6):938-945.
49. Yeh V, Bonev BB. Solid state NMR of membrane proteins: Methods and applications. Biochem Soc Trans. 2021;49(4):1505-1513.
50. Necelis M, McDermott C, Belcher Dufrisne M, Baryiames C, Columbus L. Solution NMR investigations of integral membrane proteins: Challenges and innovations. Curr Opin Struct Biol. 2023;82:102654.
51. Forest E, Man P. Conformational dynamics and interactions of membrane proteins by hydrogen/deuterium mass spectrometry. Methods Mol Biol. 2016;14 32:269-279.
52. Smits AH, Vermeulen M. Characterizing protein-protein interactions using mass spectrometry: Challenges and opportunities. Trends Biotechnol. 2016;34 (10):825-834.
53. van Dyck JF, Konijnenberg A, Sobott F. Native mass spectrometry for the characterization of structure and interactions of membrane proteins. Methods Mol Biol. 2017;1635:205-232.
54. Patrick JW, Laganowsky A. Probing heterogeneous lipid interactions with membrane proteins using mass spectrometry. Methods Mol Biol. 2019;2003:175-190.
55. Gault J, Liko I, Landreh M, Shutin D, Bolla JR, Jefferies D, Agasid M, Yen HY, Ladds MJGW, Lane DP, Khalid S, Mullen C, Remes PM, Huguet R, McAlister G, Goodwin M, Viner R, Syka JEP, Robinson CV. Combining native and 'omics' mass spectrometry to identify endogenous ligands bound to membrane proteins. Nat Methods. 2020;17(5):505-508.
56. Bolla JR, Fiorentino F, Robinson CV. Mass spectrometry informs the structure and dynamics of membrane proteins involved in lipid and drug transport. Curr Opin Struct Biol. 2021;70:53-60.
57. Keener JE, Zhang G, Marty MT. Native mass spectrometry of membrane proteins. Anal Chem. 2021;93(1):583-597.
58. Bennett JL, Nguyen GTH, Donald WA. Protein-small molecule interactions in native mass spectrometry. Chem Rev. 2022;122(8):7327-7385.
59. Ogiso H, Suno R, Kobayashi T, Kawami M, Takano M, Ogasawara M. A liquid chromatography-mass spectrometry method to study the interaction between membrane proteins and low-molecular-weight compound mixtures. Molecules. 2022;27(15):4889.
60. Yang HC, Li W, Sun J, Gross ML. Advances in mass spectrometry on membrane proteins. Membranes (Basel). 2023;13(5):457.
61. Zhu Y, Yun SD, Zhang T, Chang JY, Stover L, Laganowsky A. Native mass spectrometry of proteoliposomes containing integral and peripheral membrane proteins. Chem Sci. 2023;14 (48):14243-14255.
62. Kovachka S, Soule P, Mus-Veteau I. Microscale thermophoresis to evaluate the functionality of heterologously overexpressed membrane proteins in membrane preparations. Methods Mol Biol. 2022;2507:445-461.
63. Rascol E, Dufourquet A, Baccouch R, Soule P, Alves ID. An original approach to measure ligand/receptor binding affinity in

non-purified samples. Sci Rep. 2022;12 (1):5400.
64. Sparks RP, Lawless W, Arango AS, Tajkhorshid E, Fratti RA. Use of microscale thermophoresis to measure protein-lipid interactions. J Vis Exp. 2022;180:e60607.
65. Dijkman PM, Watts A. Lipid modulation of early G protein-coupled receptor signalling events. Biochim Biophys Acta. 2015;1848(11 Pt A):2889-2897.
66. Ormö M, Cubitt AB, Kallio K, Gross LA, Tsien RY, Remington SJ. Crystal structure of the *Aequorea victoria* green fluorescent protein. Science. 1996;273(5280):1392-13 95.
67. Remington SJ. Green fluorescent protein: A perspective. Protein Sci. 2011;20(9):1509-1519.
68. Cormack BP, Valdivia RH, Falkow S. FACS-optimized mutants of the green fluorescent protein (GFP). Gene. 1996;173(1 Spec No):33-38.
69. Cinelli RA, Ferrari A, Pellegrini V, Tyagi M, Giacca M, Beltram F. The enhanced green fluorescent protein as a tool for the analysis of protein dynamics and localization: local fluorescence study at the single-molecule level. Photochem Photobiol. 2000;71(6):771-776.
70. Petruk G, Puthia M, Petrlova J, Samsudin F, Strömdahl AC, Cerps S, et al. SARS-CoV-2 spike protein binds to bacterial lipopolysaccharide and boosts proinflammatory activity. J Mol Cell Biol. 2020;12(12):916-932.
71. Samsudin F, Raghuvamsi P, Petruk G, Puthia M, Petrlova, J, MacAry P et al. SARS-CoV-2 spike protein as a bacterial lipopolysaccharide delivery system in an overzealous inflammatory cascade. J Mol Cell Biol. 2023;14(9):mjac058.
72. Gawriljuk VO, Zin PPK, Puhl AC, Zorn KM, Foil DH, Lane TR et al. Machine learning models identify inhibitors of SARS-CoV-2. J Chem Inf Model. 2021;61(9):4224-4235.
73. Gao B, Zhu S. A fungal defensin targets the SARS-CoV-2 spike receptor-binding domain. J Fungi (Basel). 2021;7(7):553.
74. Puhl AC, Mottin M, Sacramento CQ, Tavella TA, Dias GG, Fintelman-Rodrigues N et al. Computational and experimental approaches identify beta-blockers as potential SARS-CoV-2 spike inhibitors. ACS Omega. 2022;7(32):27950-27958.
75. Song S, Shi Q. Interface-based design of high-affinity affibody ligands for the purification of RBD from spike proteins. Molecules. 2023;28(17):6358.
76. Sadremomtaz A, Al-Dahmani ZM, Ruiz-Moreno AJ, Monti Dömling A, Wang C. et al. Synthetic peptides that antagonize the angiotensin-converting enzyme-2 (ACE-2) interaction with SARS-CoV-2 receptor binding spike protein. J Med Chem. 2022;65(4):2836-2847.
77. Engelhardt PM, Florez-Rueda S, Drexelius M, Neudörfl JM, Lauster D, Hackenberger CPR et al. Synthetic α-helical peptides as potential inhibitors of the ACE2 SARS-CoV-2 interaction. Chembiochem. 2022;23 (17):e202200372.
78. Gargantilla M, Francés C, Adhav A, Forcada-Nadal A, Martínez-Gualda B, Martí-Marí O et al. C-2 thiophenyl tryptophan trimers inhibit cellular entry of SARS-CoV-2 through interaction with the viral spike (S) protein. J Med Chem. 2023;66(15):10432-10457.
79. Kim S, Liu Y, Lei Z, Dicker J, Cao Y, Zhang XF, Im W. Differential interactions between human ACE2 and spike RBD of SARS-CoV-2 variants of concern. J Chem Theory Comput. 2021;17(12):7972-7979.
80. Kim S, Liu Y, Ziarnik M, Seo S, Cao Y, Zhang XF et al. Binding of human ACE2 and RBD of Omicron enhanced by unique interaction patterns among SARS-CoV-2 variants of concern. J Comput Chem. 2023;44(4):594-601.
81. Corin K, Baaske P, Geissler S, Wienken CJ, Duhr S, Braun D et al. Structure and function analyses of the purified GPCR human vomeronasal type 1 receptor 1. Sci Rep. 2011;1:172.
82. Corin K, Baaske P, Ravel DB, Song J, Brown E, Wang X et al. Designer lipid-like peptides: a class of detergents for studying functional olfactory receptors using commercial cell-free systems. PLoS One. 2011;6(11):e25067.
83. Corin K, Baaske P, Ravel DB, Song J, Brown E, Wang X et al. A robust and rapid method of producing soluble, stable, and functional G-protein coupled receptors. PLoS One. 2011;6(10):e23036.
84. Wang X, Corin K, Baaske P, Wienken CJ, Jerabek-Willemsen M, Duhr S et al. Peptide surfactants for cell-free production of functional G protein-coupled receptors. Proc Natl Acad. Sci USA. 2011;108(22):9 049-9054.
85. Tegler LT, Corin K, Hillger J, Wassie B, Yu Y, Zhang S. Cell-free expression,

purification, and ligand-binding analysis of *Drosophila melanogaster* olfactory receptors DmOR67a, DmOR85b and DmORCO. Sci Rep. 2015;5:7867.
86. Sencanski M, Glisic S, Šnajder M, Veljkovic N, Poklar Ulrih N, Mavri J et al. Computational design and characterization of nanobody-derived peptides that stabilize the active conformation of the β2-adrenergic receptor (β2-AR). Sci Rep. 2019;9(1):16555.
87. Bada Juarez JF, Muñoz-García JC, Inácio Dos Reis R, Henry A, McMillan D, Kriek M et al. Detergent-free extraction of a functional low-expressing GPCR from a human cell line. Biochim Biophys Acta – Biomembranes. 2020;1862(3):183152.
88. Rascol E, Dufourquet A, Baccouch R, Soule P, Alves ID. An original approach to measure ligand/receptor binding affinity in non-purified samples. Sci Rep. 2022;12(1):5400.
89. Wang H, Wang P, Liang X, Li W, Yang M, Ma J et al. Down-regulation of endothelial protein C receptor promotes preeclampsia by affecting actin polymerization. J Cell Mol Med. 2020;24(6):3370-3383.
90. Brandhofer M, Hoffmann A, Blanchet X, Siminkovitch E, Rohlfing AK, El Bounkari O et al. Heterocomplexes between the atypical chemokine MIF and the CXC-motif chemokine CXCL4L1 regulate inflammation and thrombus formation. Cell Mol Life Sci. 2022;79(10):512.
91. Langelueddecke C, Roussa E, Fenton RA, Wolff NA, Lee WK, Thévenod F. Lipocalin-2 (24p3/neutrophil gelatinase-associated lipocalin (NGAL)) receptor is expressed in distal nephron and mediates protein endocytosis. J Biol Chem. 2012;287(1):1 59-169.
92. Liberelle M, Magnez R, Thuru X, Bencheikh Y, Ravez S, Quenon C et al. MUC4-ErbB2 oncogenic complex: Binding studies using microscale thermophoresis. Sci Rep. 2019;9(1):16678.
93. Bernhard M, Laube B. Thermophoretic analysis of ligand-specific conformational states of the inhibitory glycine receptor embedded in copolymer nanodiscs. Sci Rep. 2020;10(1):16569.
94. Li SY, Hou LZ, Gao YX, Zhang NN, Fan B, Wang F. FIP-nha, a fungal immunomodulatory protein from *Nectria haematococca*, induces apoptosis and autophagy in human gastric cancer cells via blocking the EGFR-mediated STAT3/Akt signaling pathway. Food Chem (Oxf). 2022;4:100091.
95. Saeed MEM, Yücer R, Dawood M, Hegazy MF, Drif A, Ooko E et al. In silico and in vitro screening of 50 curcumin compounds as EGFR and NF-κB inhibitors. Int J Mol Sci. 2022;23(7):3966.
96. Domingo IK, Groenendyk J, Michalak M, Bhavsar AP. Cisplatin toxicity is mediated by direct binding to toll-like receptor 4 through a mechanism that is distinct from metal allergens. Mol Pharmacol. 2023;103(3):158-165.
97. Powers HR, Jenjak SE, Volkman BF, Sahoo D. Development and validation of a purification system for functional full-length human SR-B1 and CD36. J Biol Chem. 2023;299(10):105187.
98. Gaur P, Seaf M, Trabelsi N, Marcu O, Gafarov D, Schueler-Furman O et al. 2B4 - A potential target in *Staphylococcus aureus* associated allergic inflammation. Clin Exp Immunol. 2024;215(1):37-46.
99. Hörnschemeyer P, Liss V, Heermann R, Jung K, Hunke S. Interaction analysis of a two-component system using nanodiscs. PLoS One. 2016;11(2):e0149187.
100. Agnarelli A, Lauer Betrán A, Papakyriakou A, Vella V, Samuels M, Papanastasopoulos P et al. The inhibitory properties of a novel, selective LMTK3 kinase inhibitor. Int J Mol Sci. 2023;24(1): 865.
101. Arbel N, Ben-Hail D, Shoshan-Barmatz V. Mediation of the antiapoptotic activity of Bcl-xL protein upon interaction with VDAC1 protein. J Biol Chem. 2012;287 (27):23152-23161.
102. Rimmerman N, Ben-Hail D, Porat Z, Juknat A, Kozela E, Daniels MP et al. Direct modulation of the outer mitochondrial membrane channel, voltage-dependent anion channel 1 (VDAC1) by cannabidiol: a novel mechanism for cannabinoid-induced cell death. Cell Death Dis. 2013;4(12):e949.
103. Smilansky A, Dangoor L, Nakdimon I, Ben-Hail D, Mizrachi D, Shoshan-Barmatz V. The voltage-dependent anion channel 1 mediates amyloid β toxicity and represents a potential target for Alzheimer disease therapy. J Biol Chem. 2015;290(52): 30670-30683.
104. Gorny H, Mularoni A, Delcros JG, Freton C, Preto J, Krimm I. Combining nano-differential scanning fluorimetry and microscale thermophoresis to investigate

VDAC1 interaction with small molecules. J Enzyme Inhib Med Chem. 2023;38(1): 2121821.
105. Ferens FG, Patel TR, Oriss G, Court DA.; Stetefeld, J. A cholesterol analog induces an oligomeric reorganization of VDAC. Biophys J. 2019;116(5):847-859.
106. Sisco NJ, Helsell CVM, Van Horn WD. Competitive interactions between PIRT, the cold sensing ion channel TRPM8, and PIP2 suggest a mechanism for regulation. Sci Rep. 2019;9(1):14128.
107. Schroder RV, Cohen LS, Wang P, Arizala JD, Poget SF. Expression, purification and refolding of a human NaV1.7 voltage sensing domain with native-like toxin binding properties. Toxins (Basel). 2021; 13(10):722.
108. Barbieri F, Bosio AG, Pattarozzi A, Tonelli M, Bajetto, A.; Verduci, I et al. Chloride intracellular channel 1 activity is not required for glioblastoma development but its inhibition dictates glioma stem cell responsivity to novel biguanide derivatives. J Exp Clin Cancer Res. 2022;41(1):53.
109. Kiya T, Takeshita K, Kawanabe A, Fujiwara Y. Intermolecular functional coupling between phosphoinositides and the potassium channel KcsA. J Biol Chem. 2022;298(298):102257.
110. Kawanabe A, Takeshita K, Takata M, Fujiwara Y. ATP modulates the activity of the voltage-gated proton channel through direct binding interaction. J Physiol. 2023;601(18):4073-4089.
111. Roche JV, Survery S, Kreida S, Nesverova V, Ampah-Korsah H, Gourdon M et al. Phosphorylation of human aquaporin 2 (AQP2) allosterically controls its interaction with the lysosomal trafficking protein LIP5. J Biol Chem. 2017;292(35):14636-14648.
112. Al-Jubair T, Steffen JH, Missel JW, Kitchen P, Salman MM, Bill RM et al. Characterization of human aquaporin protein-protein interactions using microscale thermophoresis (MST). STAR Protoc. 2022;3(2):101316.
113. He R, Su H, Wang X, Ren Z, Zhang K, Feng T et al. Coronatine promotes maize water uptake by directly binding to the aquaporin ZmPIP2;5 and enhancing its activity. J Integr Plant Biol. 2023;65(3):703-720.
114. Girke C, Arutyunova E, Syed M, Traub M, Möhlmann T, Lemieux MJ. High yield expression and purification of equilibrative nucleoside transporter 7 (ENT7) from *Arabidopsis thaliana*. Biochim Biophys Acta. 2015;1850(9):1921-1929.
115. Clémençon B, Lüscher BP, Hediger MA. Establishment of a novel microscale thermophoresis ligand-binding assay for characterization of SLC solute carriers using oligopeptide transporter PepT1 (SLC15 family) as a model system. J Pharmacol Toxicol Methods. 2018;92:67-76.
116. Majumder P, Khare S, Athreya A, Hussain N, Gulati A, Penmatsa A. Dissection of protonation sites for antibacterial recognition and transport in QacA, a multi-drug efflux transporter. J Mol Biol. 2019;431(11):2163-2179.
117. Waddad AY, Ramharack P, Soliman MES, Govender T. Grafted hyaluronic acid N-acetyl-l-methionine for targeting of LAT1 receptor: In-silico, synthesis and microscale thermophoresis studies. Int J Biol Macromol. 2019;125:767-777.
118. Shang Y, Lv P, Su D, Li Y, Liang Y, Ma C et al. Evolutionary conservative analysis revealed novel functional sites in the efflux pump NorA of *Staphylococcus aureus*. J Antimicrob Chemother. 2022;77(3):675-681.
119. Lv P, Shang Y, Zhang Y, Wang W, Liu Y, Su D et al. Structural basis for the arsenite binding and translocation of Acr3 antiporter with NhaA folding pattern. FASEB J. 2022;36(12):e22659.
120. Hussein A, Fan S, Lopez-Redondo M, Kenney I, Zhang X, Beckstein O et al. Energy coupling and stoichiometry of $Zn^{2+}/^{H+}$ antiport by the cation diffusion facilitator YiiP. eLife. 2023;12:RP87167.
121. Brown MC, Abdine A, Chavez J, Schaffner A, Torres-Arancivia C, Lada B et al. Unwinding of the substrate transmembrane helix in intramembrane proteolysis. Biophys J. 2018;114(7):1579-1589.
122. Heybrock S, Kanerva K, Meng Y, Ing C, Liang A, Xiong ZJ et al. Lysosomal integral membrane protein-2 (LIMP-2/SCARB2) is involved in lysosomal cholesterol export. Nat Commun. 2019;10(1):3521.
123. Huang C, Hays FA, Tomasek JJ, Benyajati S, Zhang XA. Tetraspanin CD82 interaction with cholesterol promotes extracellular vesicle-mediated release of ezrin to inhibit tumour cell movement. J Extracell Vesicles. 2019;9(1):1692417.
124. Sisco NJ, Luu DD, Kim M, Van Horn WD. PIRT the TRP channel regulating protein

binds calmodulin and cholesterol-like ligands. Biomolecules. 2020;10(3):478.
125. Srivastava AK, Venkata BS, Sweat YY, Rizzo HR, Jean-François L, Zuo L et al. Serine 408 phosphorylation is a molecular switch that regulates structure and function of the occludin α-helical bundle. Proc Natl Acad Sci U A. 2022;119(34):e2204618119.
126. Naneh O, Kozorog M, Merzel F, Gilbert R, Anderluh G. Surface plasmon resonance and microscale thermophoresis approaches for determining the affinity of perforin for calcium ions. Front Immunol. 2023;14:1181020.
127. Nolden KA, Harwig MC, Hill RB. Human Fis1 directly interacts with Drp1 in an evolutionarily conserved manner to promote mitochondrial fission. J Biol Chem. 2023;299(12): 105380.

Peer-review history:
The peer review history for this paper can be accessed here:
https://www.sdiarticle5.com/review-history/113143